The distribution of red and blue galaxies in groups: an empirical test of the halo model

Adrian A. Collister^{1*}, Ofer Lahav²

- ¹ Institute of Astronomy, University of Cambridge, Cambridge CB3 0HA, UK
- ² Department of Physics and Astronomy, University College London, Gower Street, London WC1E 6BT, UK

ABSTRACT

The popular halo model predicts that the power spectrum of the galaxy fluctuations is simply the sum of the large scale linear halo-halo power spectrum and the weighted power spectrum of the halo profile. Previous studies have derived halo parameters from the observed galaxy correlation function. Here we test the halo model directly for self-consistency with a minimal set of theoretical assumptions by utilising the 2dF Galaxy Redshift Survey (2dFGRS). We derive empirically the halo occupation and galaxy radial distributions in the haloes of the 2dF Percolation-Inferred Galaxy Group (2PIGG) catalogue. The mean halo occupation number is found to be well-fitted by a power-law, $\langle N|M\rangle \propto M^{\beta}$, at high masses, with $\beta = 1.05, 0.88, 0.99$ for red, blue and all galaxies respectively (with 1-sigma errors of 15-19%). We find that the truncated NFW profile provides a good fit to the galaxy radial distributions, with concentration parameters c = 3.9, 1.3, 2.4 for red, blue and all galaxies respectively (with 1-sigma errors of 8-15%). Adding the observed linear power spectrum to these results, we compare these empirical predictions of the halo model with the observed correlation functions for these same 2dF galaxy populations. We conclude that subject to some fine tuning it is an acceptable model for the two-point correlations. Our analysis also explains why the correlation function slope of the red galaxies is steeper than that of the blue galaxies. It is mainly due to the number of red and blue galaxies per halo, rather than the radial distribution within the haloes of the two galaxy species.

Key words: large-scale structure of Universe – galaxies: haloes – galaxies: statistics – dark matter

1 INTRODUCTION

It is well known that galaxies of different types are not identically distributed within galaxy groups (manifested in the well-known phenomenon of morphological segregation, e.g. Dressler 1980; Postman & Geller 1984; Goto et al. 2003). Red, typically elliptical galaxies, with low star-formation rates are preferentially found towards the centres of large groups, while blue, actively star-forming galaxies dominate in the outskirts of groups and in the field. Furthermore, measurements of the galaxy-galaxy two-point correlation function have shown that it is well fitted by a power-law over a wide range of distance scales (e.g. Peebles 1980; Zehavi et al. 2002; Hawkins et al. 2003), and that the slope of this powerlaw is a function of galaxy spectral type or colour (e.g. Zehavi et al. 2002; Norberg et al. 2002a; Madgwick et al. 2003): blue galaxies have a shallower two-point correlation function than the red galaxies. The correlation function of the dark matter, on the other hand, has a lower amplitude

and is far from being a featureless power-law, thus the galaxy distribution is said to be biased with respect to the dark matter.

Much recent progress towards understanding the nature of galaxy biasing has come through use of the halo model of large scale structure. The model has its origins in the work of Neyman & Scott (1952), and was first applied to continuous density fields by Scherrer & Bertschinger (1991). It has been recently used in the context of the clustering of both dark matter and galaxies (e.g. Peacock & Smith 2000; Seljak 2000: Scoccimarro et al. 2001: Berlind & Weinberg 2002: Magliocchetti & Porciani 2003; van den Bosch, Yang & Mo 2003). Cooray & Sheth (2002) provide a detailed review. In the model, matter in the universe is assumed to reside only in discrete haloes. The distribution of the matter within the haloes gives rise to the non-linear component of the power spectrum, while the large-scale distribution of the haloes in space is responsible for the power on linear scales. The simplicity of the model allows analytic calculations of correlation functions to be made, so that large parameter spaces can be investigated at relatively little cost when compared to numerical simulations of the large scale structure.

Two ingredients are required to extend the model to galaxy clustering: the probability distribution for the number of galaxies hosted by a particular halo, P(N|M), known as the halo occupation distribution (HOD), and the spatial distribution of galaxies within haloes. The distribution of the galaxies within haloes is commonly assumed, ad hoc, to be the same as that of the dark matter; differences in the clustering properties are then solely due to the choice of halo occupation distribution. We do not rely on this assumption in our analysis below, but instead obtain the actual galaxy group radial density distributions observationally. This allows us to confirm, for observed HODs and radial profiles, the findings of Sheth et al. (2001), who used HODs drawn from semi-analytic models to demonstrate the dominance of the HOD over the intra-halo distribution in the correlation function.

Previous studies have assumed the validity of the halo model, and used the observed galaxy correlation functions to constrain the halo occupation distribution, or the radial distribution of galaxies in haloes (e.g. Magliocchetti & Porciani 2003; Scranton 2003; van den Bosch et al. 2003). In contrast, we take as empirical an approach as possible. We directly measure the radial and halo occupation distributions of galaxies in the 2dFGRS Percolation-Inferred Galaxy Group (2PIGG) catalogue (Eke et al. 2004a), focusing in particular on the separate distributions of red and blue galaxies. Having measured these distributions, no free parameters remain in the model. Since the correlation functions of these populations have previously been directly obtained (Norberg et al. 2002a; Hawkins et al. 2003; Madgwick et al. 2003), the non-trivial success of the halo model in reproducing the observed clustering statistics can be directly tested using fully self-consistent 2dF observations. Requiring the model to account for the differences in the observed correlation functions of the red and blue populations is an especially stringent test.

The structure of this paper is as follows. In Section 2 we describe the halo model in detail. We introduce the 2PIGG catalogue in Section 3 and describe how the properties of interest are inferred from the observational data. In Section 4 the halo occupation distribution is investigated, and in Section 5 we examine the radial distribution of galaxies within the 2PIGGs. Finally, in Section 6, the halo model is applied to our results, and the predicted clustering results compared with observations.

2 THE HALO MODEL FORMALISM

In essence, the halo model exemplifies the natural distinction between linear (large-scale) and non-linear (small-scale) clustering. Indeed, the two regimes appear as separate terms in the halo model galaxy power spectrum:

$$P_{\rm gal}(k) = P_{\rm gal}^{(1h)}(k) + P_{\rm gal}^{(2h)}(k),$$
 (1)

with $P_{\rm gal}^{(1{\rm h})}(k)$ the *intra*-halo, non-linear term, and $P_{\rm gal}^{(2{\rm h})}(k)$ the *inter*-halo, linear term. Although we will later require the two-point correlation functions, $\xi(r)$, explicit calculation of these involves convolutions of the halo profiles; we prefer

instead to work in Fourier space, ultimately obtaining the correlation function via the transform

$$\xi_{\rm gg}(r) = \int \Delta_{\rm gal}^2(k) \frac{\sin(kr)}{kr} \frac{\mathrm{d}k}{k},\tag{2}$$

with $\Delta_{\rm gal}^2(k) = \frac{k^3}{2\pi^2} P_{\rm gal}(k)$, the dimensionless form of the power spectrum.

Within the halo model framework, the components of the galaxy power spectrum are (e.g. Cooray & Sheth 2002)

$$P_{\text{gal}}^{(1\text{h})}(k) = \int dM \ n(M) \frac{\langle N(N-1)|M\rangle}{\bar{n}_{\text{gal}}^2} |\hat{u}_{\text{gal}}(k|M)|^2, \quad (3)$$

and

$$P_{\rm gal}^{\rm (2h)}(k) = P_{\rm dm}^{\rm (lin)}(k) \left[\int \mathrm{d} M n(M) b(M) \frac{\langle N|M\rangle}{\bar{n}_{\rm gal}} \hat{u}_{\rm gal}(k|M) \right]^2, (4)$$

where the integrals are over the halo mass, M. In these expressions, n(M) is the halo mass function, b(M) is the halo biasing factor, $\langle N|M\rangle$ and $\langle N(N-1)|M\rangle$ are the first and second factorial moments of the halo occupation distribution, P(N|M), respectively, $\bar{n}_{\rm gal}$ is the average number density of galaxies, and $\hat{u}_{\rm gal}(k|M)$ is the Fourier transform of the normalised radial distribution of galaxies within haloes. The following sections describe these terms in more detail.

In keeping with the ethos of this work, we opt to use the simplest possible implementation of the halo model. We note for completeness that the implementation may be modified to account for the expectation that the first galaxy in each halo resides at the halo centre of mass (see e.g. Cooray & Sheth 2002; Kravtsov et al. 2004).

2.1 Halo mass function

The number density of haloes of mass M in space is described by the mass function, n(M), which we assume to have the form proposed by Sheth & Tormen (1999) (an extension of the Press & Schechter (1974) form):

$$n(M)dM = \frac{\bar{\rho}}{M}f(\nu)d\nu, \tag{5}$$

$$\nu f(\nu) = A_* \left(1 + (q\nu)^{-p} \right) \left(\frac{q\nu}{2\pi} \right)^{1/2} e^{-q\nu/2},$$
 (6)

where $\bar{\rho}$ is the background density of the universe, q=0.707, p=0.3, and normalisation implies $A_*\approx 0.3222$. The mass variable is defined as $\nu\equiv (\delta_{\rm sc}(z)/\sigma(M))^2$, where $\delta_{\rm sc}(z)$ is the linear-theory prediction for the present day overdensity of a region undergoing spherical collapse at redshift z, and $\sigma(M)$ is the r.m.s. variance of the present day linear power spectrum in a spherical top-hat which contains an average mass M. Note that the mass function depends on the redshift only through $\delta_{\rm sc}(z)=\delta_{\rm sc}(0)/D(z)$, where $\delta_{\rm sc}(0)\approx 1.68$, and D(z) is the linear growth factor, normalized so that D(0)=1. The value of $\delta_{\rm sc}(0)$ is only weakly sensitive to the cosmological model (Eke, Cole & Frenk 1996).

2.2 Halo biasing

Haloes are biased tracers of the overall dark matter distribution. The degree of bias is a function of the halo mass. Following Mo & White (1996), we can write the power spectrum of dark matter haloes of given masses, M_1 and M_2 as

$$P_{\rm hh}(k; M_1, M_2) = b(M_1) \ b(M_2) \ P_{\rm dm}(k). \tag{7}$$

We further assume $P_{\rm dm}(k)=P_{\rm dm}^{\rm (lin)}(k)$, the linear dark matter power spectrum, since inter-halo correlations are only important on large, quasi-linear scales. Sheth & Tormen (1999) derive the required halo bias factors,

$$b(M) = 1 + \frac{q\nu - 1}{\delta_{sc}(z)} + \frac{2p/\delta_{sc}(z)}{1 + (q\nu)^p}.$$
 (8)

with p and q taking the values given in Section 2.1.

2.3 Galaxy distribution

The halo occupation distribution, P(N|M), appears in the power spectrum (equations 3 and 4) through its first and second factorial moments, $\langle N|M\rangle$ and $\langle N(N-1)|M\rangle$ respectively. The galaxy number density is given by

$$\bar{n}_{\text{gal}} = \int \langle N|M\rangle \, n(M) \, dM.$$
(9)

The spatial distribution of galaxies within haloes is assumed to be spherically symmetric about the halo centre, so that the density profile, $\rho_{\rm gal}(r|M)$, is a function of r only for a halo of a given mass M. The profile is normalized so that $\int_0^{r_{\rm vir}} \hat{\rho}_{\rm gal}(r|M) \ 4\pi r^2 {\rm d}r = 1 \ (r_{\rm vir}$ will be defined in equation 13), and the Fourier transform of the normalized profile is denoted by $\hat{u}_{\rm gal}(k|M)$.

We attempt to directly measure the radial density and halo occupation distributions in subsequent sections.

2.4 Galaxy bias

On distance scales for which the inter-halo term is important, $u_{\rm gal}(k|M)\approx 1$ is a good approximation. The integral on the right-hand side of equation 4 is then independent of scale and we can re-write the relations as:

$$P_{\rm gal}^{(2h)}(k) = b_{\rm gal}^2 P_{\rm dm}^{({\rm lin})}(k),$$
 (10)

where we have defined the galaxy bias parameter as:

$$b_{\rm gal} \equiv \int dM \ n(M) \ b(M) \frac{\langle N|M\rangle}{\bar{n}_{\rm gal}}. \tag{11}$$

2.5 An empirical approach to the halo model

As we have stressed, our aim is to rely on observations wherever possible, avoiding model-dependent assumptions. Our underlying assumption is that the observed galaxy groups represent the haloes. Even if this assumption is not perfect it is very likely that there is a simple ranking relation between the observed galaxy groups and the underlying dark matter haloes. Although we could take for n(M) the histogram of the observed groups versus their estimated mass, we prefer to use the more robust mass function n(M) given by equation 5. Future group samples with accurate masses will allow us to use them directly for n(M).

Equation 3 requires knowledge of the occupation quantities $\langle N|M\rangle$, $\langle N(N-1)|M\rangle$ and the radial profile $\rho_{\rm gal}(r)$ which we shall determine directly from the 2PIGG sample per galaxy type. The mean number of galaxies (equation 9) then follows from the above n(M) and $\langle N|M\rangle$.

The halo-halo correlation power spectrum $P_{\mathrm{gal}}^{(2\mathrm{h})}(k)$

could in principle be taken directly from the group-group power spectrum. The group-group correlation functions have actually been derived by Padilla et al. (2004) and Yang et al. (2005b). However, biases in mapping the groups to haloes may make this approach somewhat inaccurate with the present data. While this should be possible with future group samples here we follow the approximation given by equations 10 and 11. In fact, as shown later in Section 6.1, we find that $b_{\rm gal}$ is close to unity, interestingly in accord with the biasing derived from the 2dF linear galaxy-galaxy power spectrum (Percival et al. 2001) combined with pre-WMAP CMB measurements (Lahay et al. 2002). In practice we use equations 10 and 11 with the linear power spectrum of the dark matter, $P_{\rm dm}^{\rm (lin)}(k)$, which has been well constrained by observations of the Cosmic Microwave Background (CMB). The galaxy power spectrum on linear scales has also been measured observationally, for example by Percival et al. (2001) from the 2dFGRS, and Tegmark et al. (2002) from the Sloan Digital Sky Survey. The shapes of these power spectra have been shown to be consistent with a flat universe Λ -CDM matter power spectrum, with present epoch $\Omega_{\rm m} \sim 0.3$ (Percival et al. 2001; Efstathiou et al. 2002; Cole et al. 2005). We therefore assume this form for $P_{\mathrm{dm}}^{(\mathrm{lin})}(k)$, adopting the WMAP normalisation $\sigma_8 = 0.9$ (Spergel et al. 2003) and the biasing parameter derived in Section 6.1.

We emphasize again that although we have to compromise here by making several theoretical assumptions, it would be possible in the future to use galaxy and group catalogues to test the halo model almost without any theoretical prior.

3 GALAXY GROUP CATALOGUE

We assume that galaxy groups are representative of the underlying dark matter haloes. The 2dFGRS Percolation-Inferred Galaxy Group catalogue (2PIGG; Eke et al. 2004a) is currently the largest homogeneous sample of galaxy groups publicly available. It comprises $\sim 29,000$ groups containing at least two galaxy members, which host a total of $\sim 105,000$ galaxies. As described in the following subsections, we apply a number of cuts to the catalogue in order to improve the quality of the sample used in our analyses (our final sample comprises ~ 3000 groups).

An independent attempt at constructing a galaxy group catalogue for the 2dFGRS has been made by Yang et al. (2005a), using a halo model-based algorithm. Although it is not the aim of this work to perform a comparative study of the two catalogues we note relevant differences where appropriate.

The 2PIGG groups were identified from the 2dFGRS by means of a friends-of-friends (FOF) percolation algorithm. Eke et al. (2004a) tested the algorithm on mock samples generated from cosmological dark matter simulations in order to optimize the mapping between the recovered galaxy groups and the actual dark matter haloes; this strengthens the case for our prior assumption that galaxy groups may be identified with the true bound structures in the dark matter distribution.

Eke et al. (2004a) tuned their group-finding algorithm so as to maximize the completeness of the recovered groups.

Consequently, very few true group members are erroneously excluded, but this is at the expense of increased contamination by interlopers (i.e. field galaxies assigned to groups, or false groups comprised entirely of field galaxies). The severity of the contamination increases with redshift; following Eke et al. (2004b), we discard groups at redshifts greater than z=0.12. At this redshift the total number of field galaxies included in groups rises to ~ 50 per cent of the total number of true group members, and the number of interlopers increases very rapidly with redshift beyond this point. This cut leaves $\sim 16,000$ remaining groups. We note that the halo-based group finder of Yang et al. (2005a) achieves similar completeness to standard FOF but reduces the contamination level, typically by a factor of two (for group masses $M \gtrsim 10^{14} h^{-1} {\rm M}_{\odot}$).

3.1 Spectral classification

Madgwick et al. (2002) used a principal component analysis of the 2dFGRS dataset to define, η , a continuous parametrization of spectral type. This parameter is most strongly correlated with the current star formation rate in each galaxy, but is also a good indicator for morphological type and colour. Following Madgwick et al. (2003), we broadly classify galaxies in our sample using a cut at $\eta = -1.4$. We label galaxies with $\eta > -1.4$ (relatively active) as blue galaxies, and those with $\eta < -1.4$ (relatively passive) as red. We exclude from our analysis any group which does not have a measurement of η for all its member galaxies. This reduces the sample to $\sim 14,000$ groups.

3.2 Mass estimation

The majority of the 2PIGGs have a measurement for the one-dimensional velocity dispersion, $\sigma_{\rm v}$. This can be used to estimate the group mass as

$$M = A \frac{\sigma_{\rm v}^2 R_{\rm rms}}{G},\tag{12}$$

where $R_{\rm rms}$ is the r.m.s. projected separation from the central galaxy of the remaining galaxies assigned to the group. Through use of simulated mock surveys, Eke et al. (2004a) derive the value A=5.0 by requiring that the estimated mass be unbiased with respect to that of the underlying dark matter haloes. The simulated dark matter haloes are identified using a friends-of-friends algorithm, and the recovered haloes have mean spherical overdensities of ~ 200 times the background density (Eke, private communication). Sheth & Tormen (1999) define the mass of a halo to be that enclosed within such an overdensity, thus it is valid to identify the mass estimate of equation 12 with the halo mass used throughout Section 2.

The measurement of the velocity dispersion is very unreliable for groups with a small number of observed galaxies, and even for groups with large memberships we must be wary of the significant scatter in the relation between group mass and the velocity dispersion (see fig. 3 of Eke et al. 2004b). Yang et al. (2005a) have independently constructed a galaxy group catalogue for the 2dFGRS. They investigate the reliability of dynamical mass estimates, and propose an alternative halo mass assignment based on total group luminosity. This gives them a particular advantage at low group

masses where the dynamical masses are especially unreliable.

To avoid the poorest mass estimates we retain only those groups with at least four observed galaxy members. The final sample contains 3,147 groups hosting a total of 25,118 galaxies (of which 12,851 are blue and 12,267 are red).

In order to maintain internal consistency regarding the definition of the group mass, we define the group virial radius.

$$r_{\rm vir} = \left(\frac{3M}{4\pi\Delta\bar{\rho}}\right)^{\frac{1}{3}},\tag{13}$$

to be that enclosing a spherical overdensity $\Delta=200$ times the background density of the universe (at the group redshift).

3.3 Group membership

In order to estimate the true galaxy membership of the 2PIGGs it is necessary to correct for (i) the flux limit, and (ii) the incompleteness of the 2dF survey due to e.g. constraints on fibre positioning. Eke et al. (2004a) compute for each galaxy a weight, $w_j \geq 1$, to account for the local incompleteness of the survey. These weights only account for missed galaxies which are brighter than the local magnitude limit, $b_{\rm J,lim}$; the flux limit is not yet accounted for.

In order for the group membership to be well-defined observationally, a limiting absolute magnitude, $M_{b_{\rm J},{\rm com}}$, must be specified. We explain in Section 6 how our choices for this limit are dictated by the samples used in determining the observed correlation functions; the values we use are $M_{b_{\rm J},{\rm com}}-5\log_{10}h=-19.25,-19.04,-19.50$ for red, blue and all galaxies respectively.

The faintest detectable absolute magnitude at distance x is given by $M_{b_{\rm J}}^{(i)}(x)=b_{\rm J,lim}-25-5\log(x)-K^{(i)}(x)$ for galaxies of spectral type i, where $K^{(i)}(x)$ is the K-correction (measured for each spectral type by Madgwick et al. 2002). Of all the galaxies more luminous than the threshold $M_{b_{\rm J},\rm com}$, the fraction which are detectable at distance x is given by the selection function:

$$\varphi^{(i)}(x) = \frac{\int_{-\infty}^{M_{bJ}^{(i)}(x)} \phi^{(i)}(M) \, dM}{\int_{-\infty}^{M_{\text{max}}} \phi^{(i)}(M) \, dM}, \tag{14}$$

where $M_{\text{max}} = \max(M_{b_{\text{J}}}^{(i)}(x), M_{b_{\text{J}},\text{com}})$. A further complication is that galaxies with $b_{\text{J}} < 14$ were removed from the redshift catalogue; the lower integration limit of the numerator in equation 14 is adjusted to account for this.

Since we are dealing with galaxies in groups we choose to use luminosity functions (LFs) specific to the populations of these over-dense regions, rather than those of the whole 2dF sample. Croton et al. (2005) have derived 2dF LFs as a function of density environment and per spectral type. We use their 'cluster' LFs for red and blue galaxies to compute the selection function for the 2PIGGs.

We can now assign to each galaxy a weight w'_j , which accounts for both the local incompleteness and the luminosity and flux limits. This weight is defined as

$$w'_{j} = \begin{cases} w_{j}/\varphi^{(i)}(x) & (M_{b_{J}} < M_{b_{J},com}) \\ 0 & (M_{b_{J}} > M_{b_{J},com}) \end{cases}$$
 (15)

for a galaxy of spectral type i hosted by a group at distance x, where $M_{b_{\rm J}}$ is the absolute magnitude of the galaxy in question. The galaxy membership of a group, complete to the absolute magnitude limit, may finally be obtained by summing these weights over the galaxies assigned to the group.

4 HALO OCCUPATION DISTRIBUTION

Having estimated the group membership as described in Section 3.3, we calculate the mean halo occupation numbers as a function of group mass (Figs 1 and 2). The error bars on these points are purely statistical: the uncertainty in the mass estimates is not directly accounted for. Berlind & Weinberg (2002) have used simulated galaxy group data to gauge the impact of this dispersion on the determination of $\langle N|M\rangle$. Amongst their conclusions they find:

- (i) The exclusion of groups with fewer than four observed members is responsible for $\langle N|M\rangle$ being systematically overestimated at low masses $(M\lesssim 10^{14}h^{-1}{\rm M}_{\odot}).^1$
- (ii) At higher masses, the measured amplitude is likely to be biased relative to the true value. This is due to the decrease in group abundance with increasing mass: of the groups scattered into a particular mass range, the majority originate from lower masses (and therefore have a lower average occupation number).
- (iii) Despite the scatter, the recovered slope at high group masses is not significantly biased (for sufficiently steep $\langle N|M\rangle$; see below).

In the particular case of the 2PIGG catalogue, the impact of (ii) will be countered by the relatively high number of interlopers (these competing effects are of a roughly similar magnitude). Furthermore, we note that equations 3 and 4 do not directly depend on the amplitude of $\langle N|M\rangle$ since $\bar{n}_{\rm gal}$ scales identically, so the expected bias in our measurement is not a great concern in this context (but see Section 4.2).

Semi-analytic models (e.g. Benson et al. 2000; Sheth & Diaferio 2001) unanimously predict that $\langle N|M\rangle$ should tend to a power-law at high masses. The behaviour at low masses is expected to be somewhat more complicated, particularly when the occupation numbers of red and blue sub-populations are considered separately. Unfortunately, as Berlind & Weinberg (2002) predict, we are unable to reliably probe the halo occupation distribution for masses less than $\sim 10^{14}h^{-1}{\rm M}_{\odot}$. In the interests of keeping our results as empirical as possible, we therefore adopt the simplest possible model for the mean occupation number: a single power-law with a cut-off at low mass. Thus,

$$\langle N|M\rangle = \begin{cases} (M/M_0)^{\beta} & (M \geqslant M_{\text{cut}})\\ 0 & (M < M_{\text{cut}}) \end{cases}$$
 (16)

where M_0 and β are free parameters. Berlind & Weinberg

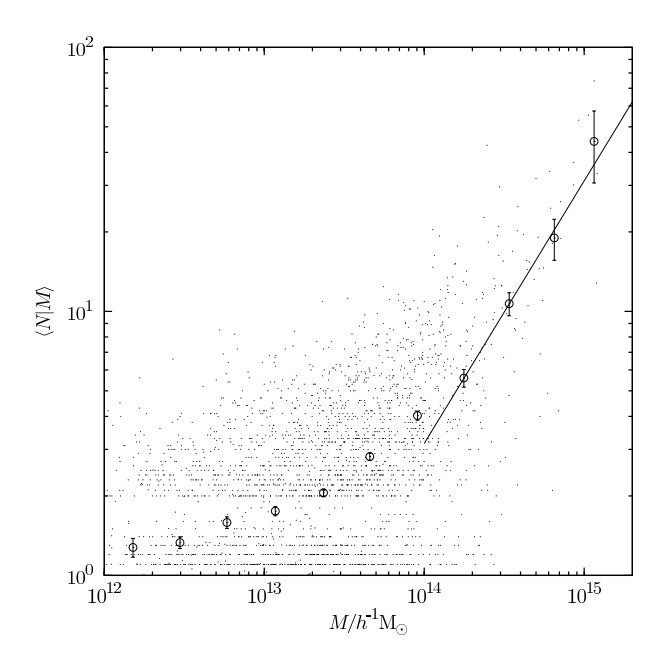


Figure 1. Total galaxy occupancy of 2PIGGs (above the minimum absolute magnitude limit $M_{b_{\rm J,com}}-5\log_{10}h=-19.50$). Points represent the individual groups used in the analysis. Open circles show the average occupancy in bins of the group mass, with 1-sigma statistical errors. The dashed line shows the best-fitting power-law (see Table 1). The fitting was performed only over the range $M>10^{14}h^{-1}{\rm M}_{\odot}$ since our exclusion of groups with fewer than four observed members means that we expect to systematically overestimate the halo occupation for less massive groups.

(2002) suggest that β may be reliably recovered, despite the dispersion in the mass, for $\beta \gtrsim 0.7$.

Using only the data for groups with $M>10^{14}h^{-1}{\rm M}_{\odot}$, we have fitted power-laws to the measured mean occupation numbers; the best-fitting parameters are given in Table 1 and the fits are overlaid on the results in Figs 1 and 2. In this high mass limit the power-law provides a good fit. We find $\beta>0.7$ for all three samples, so these estimates of the high-mass slope ought not to be seriously affected by the scatter in the mass.

Our results for the power-law slope at high group masses are in good agreement with previous work. For example, Sheth & Diaferio (2001) make simple fits to the semi-analytic models of Kauffmann et al. (1999) and find power-laws with $\beta_{\rm red}=0.9$ and $\beta_{\rm blue}=0.8$ (but note that their definitions of 'red' and 'blue' differ from ours). Magliocchetti & Porciani (2003) use the observed 2dF correlation functions to constrain the HOD. They use the same cut on η (see Section 3.1) to define red and blue populations, and find for their best-fitting models $\beta_{\rm red}=1.1^{+0.1}_{-0.2}$ and $\beta_{\rm blue}=0.7^{+0.2}_{-0.1}$ in the high-mass limit.

4.1 Second moment

The second moment $\langle N(N-1)|M\rangle$ of P(N|M) is usually expressed in terms of the parameter $\alpha(M)$, where

$$\langle N(N-1)|M\rangle = \alpha^2(M) \langle N|M\rangle^2. \tag{17}$$

 $^{^1}$ Note that, after the imposition of the absolute magnitude limits, $M_{b_{\rm J},{\rm com}},$ our sample does in fact include groups with fewer than four members.

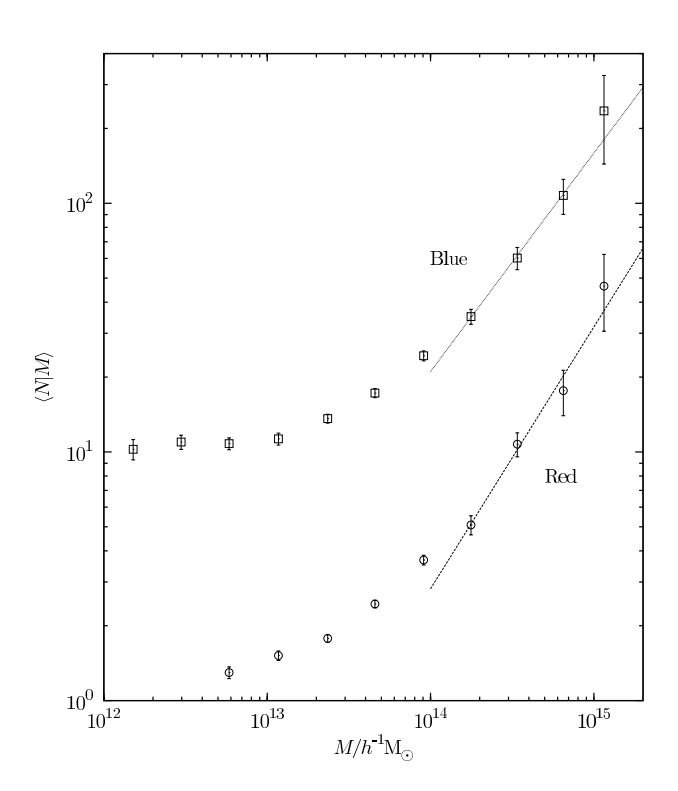


Figure 2. As Fig. 1, but showing separately the mean occupation numbers for blue and red galaxies (for clarity, the results for blue galaxies have been translated up one decade, and individual groups are not plotted).

Table 1. Best-fitting parameters to $\langle N|M\rangle=(M/M_0)^\beta$. Errors are 1-sigma, marginalized over the other fitted parameter in each case.

| | $\log(M_0/h^{-1}\mathrm{M}_{\odot})$ | β |
|-----------------------------|---|--|
| All galaxies Red Blue | $13.50^{+0.13}_{-0.19} \\ 13.57^{+0.13}_{-0.18} \\ 13.63^{+0.13}_{-0.18}$ | $0.99_{-0.17}^{+0.15} \\ 1.05_{-0.19}^{+0.17} \\ 0.88_{-0.17}^{+0.16}$ |

A pure Poisson distribution has $\alpha(M)=1$, but semi-analytic models suggest that in fact P(N|M) has a sub-Poisson distribution, i.e. $\alpha(M)<1$, particularly at low halo masses. Kravtsov et al. (2004) and Casas-Miranda et al. (2002) discuss models for the sub-Poissonian behaviour of the HOD.

We directly measure $\langle N(N-1)|M\rangle$ from the 2PIGG data and show the results in Fig. 3 (in the form of α). Contrary to expectations we find $\alpha(M)>1$ across the entire mass range for all galaxy types: averaged over all masses, $\alpha=1.17\pm0.06, 1.16\pm0.06, 1.13\pm0.05$ for red, blue and all galaxies respectively. This is undoubtedly an effect of the dispersion in the mass estimates: $\langle N(N-1)|M\rangle$ describes the width of P(N|M), but the large scatter in the mass leads to a broadening of the observed distribution and hence an overestimate of $\langle N(N-1)|M\rangle$. It is especially difficult to obtain masses for low-mass, low-occupancy groups, and

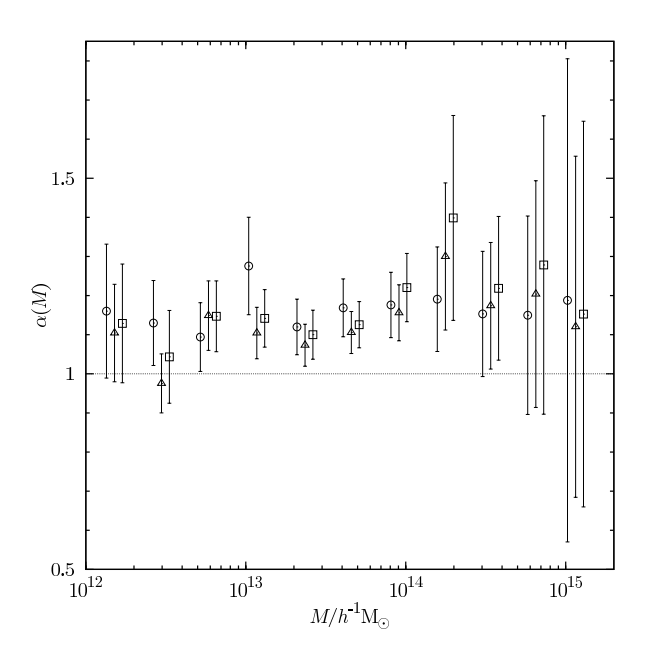


Figure 3. Measured values of $\alpha(M)$ (defined in equation 17), for blue (circles), red (squares), and all galaxies (triangles). For clarity, points for blue and red galaxies are displaced slightly either side of the true bin mass.

it is therefore neither surprising nor significant that we do not observe the expected sub-Poissonian behaviour in this regime. Our measured $\alpha(M)$ can thus only be considered as an upper limit. Guided by our observations, and in the interests of simplicity we assume $\alpha(M)=1$ for all halo masses when calculating correlation functions in Section 6. We note that Yang et al. (2005c), using their alternative mass determination, do find the expected sub-Poissonian behaviour for low-mass groups.

4.2 Extrapolation to low mass

As we mention above, observational difficulties mean we are unable to recover the halo occupation distribution for haloes less massive than around $10^{14} h^{-1} \rm M_{\odot}$. In particular, we cannot directly determine the minimum halo mass, $M_{\rm cut}$, which may host a galaxy. However, under the assumption that the HOD is well described by equation 16, the one remaining free parameter, $M_{\rm cut}$, can be constrained by requiring that we recover the correct average space density of galaxies.

The actual (observed) galaxy number density may be obtained directly from the luminosity function (integrated over the range of luminosity required); for this purpose we use the 2dF luminosity functions per type (regardless of environment) of Madgwick et al. (2002). $M_{\rm cut}$ can then be constrained by requiring that equation 9 agrees with this observed value.

The values we obtain for $M_{\rm cut}$ through this method are unphysically low (in fact, for the combined and red samples it is not possible to match the observed number density even by allowing $M_{\rm cut}=0$). This might be attributed in part to the underestimation of the amplitude of $\langle N|M\rangle$ predicted by Berlind & Weinberg (2002), but is most likely due to the overly simplistic HOD we have adopted (equation 16). It is

Table 2. Galaxy number densities (for galaxies brighter than the absolute magnitude limits derived in Section 6) computed from the luminosity functions of Madgwick et al. (2002). The quoted 1-sigma errors are estimated from the uncertainties in the parameters of the luminosity functions.

| | $\bar{n}_{\rm g} \ (10^{-3} h^3 {\rm Mpc}^{-3})$ |
|--------------|--|
| All galaxies | 5.06 ± 0.49 |
| Red | 3.90 ± 0.35 |
| Blue | 4.80 ± 0.27 |

more usual to have $\langle N|M\rangle$ tend asymptotically to unity at low mass (e.g. Kravtsov et al. 2004), significantly increasing the number of galaxies hosted by haloes in this mass range relative to the pure power-law we have adopted. We consider the impact of these issues on the halo model correlation functions in Section 6.2. For the purposes of Section 6 we adopt $M_{\rm cut}=0$ when using the simple power-law HOD (equation 16).

5 RADIAL DISTRIBUTION OF GALAXIES IN GROUPS.

We wish to obtain the group galaxy density profile given the group mass: $\rho_{\rm gal}(r|M)$. Unfortunately the virial motions of galaxies in groups give rise to redshift distortions (e.g. the so-called fingers-of-god), so that redshift information alone is not suitable for determining the three-dimensional galaxy distribution in groups. We can therefore only measure the surface density projected along the line-of-sight, $\Sigma_{\rm gal}(R)$ (where the upper-case R denotes projected distance from the group centre). Only if spherical symmetry is assumed can we unambiguously infer $\rho_{\rm gal}(r|M)$ from $\Sigma_{\rm gal}(R)$.

Eke et al. (2004a) systematically label one member of each 2PIGG as the central galaxy. For each group we calculate the projected angular separation from the central galaxy of the remaining group members. Unfortunately, even for the richest groups, there are insufficent galaxies to allow the radial distribution to be recovered with reasonable signalto-noise for an individual group. We therefore scale the projected separations in each group by its virial radius to allow like-for-like stacking of groups over a range of masses. The total surface density of galaxies is then calculated by summing the weights w'_i in radial bins. Summing the weights ensures that the profile is correctly normalized; although the actual value of the amplitude is of no consequence in the context of the halo model, it is interesting to compare the relative number densities of red and blue galaxies as a function of radius. We find that the shape of the profile is not altered if we use a simple number count instead of summing the weights. Futhermore, the shape of the profile is also found to be insensitive to the limiting absolute magnitude used and we therefore choose to use a considerably fainter limit, $M_{b_1,\text{com}} - 5\log_{10} h = -17.5$, than used to determine the group membership, so as to increase the number of galaxies admitted and hence improve the statistics.

The design of the 2dF spectrograph means that fibres cannot be positioned within $\sim 30''$ of one another, hence there is effectively an exclusion zone of this angular radius around the central galaxy in each group. Furthermore,

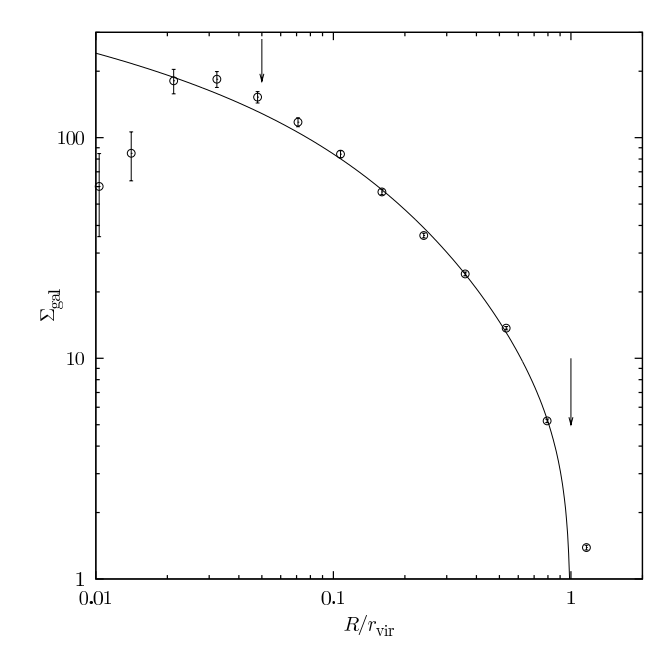


Figure 4. Projected galaxy density profile from stacking all groups in our sample, scaled by their respective virial radii. The best-fitting NFW profile (c=3.4) is overlaid. The decline in surface density within $R\lesssim 0.05~r_{\rm vir}$ is due to close-pair incompleteness; the angular diameter selection described in the text ensures that its influence is confined to this region for all the groups included in this composite profile. Arrows indicate the radial range over which the profile fitting was performed.

such close-pair incompleteness also exists in the 2dF's parent APM catalogue; van den Bosch et al. (2005) show that these have an equally important impact on the measured surface density at small separations. The severity of the problem is a decreasing function of the apparent angular size of a group. We have therefore imposed an additional selection on the sample used in this section, discarding all groups having a virial angular diameter less than 600". Since fibre collisions occur on angular scales $\lesssim 30''$, this confines the affected region to projected separations from the group centre of $R \lesssim 0.05~r_{\rm vir}.$ This choice of cut-off optimizes the balance between the increased statistical noise resulting from using fewer groups, and the improved constraints on the profile shape achieved by probing nearer to the centre. The remaining sample comprises 1,619 groups containing a total of 16,749 galaxies.

The observed surface density profiles are shown in Fig. 4 for all galaxy types, and in Fig. 5 for blue and red galaxies separately. The decline in surface density due to close-pair incompleteness in the region $R \lesssim 0.05~r_{\rm vir}$ is very apparent. We note also that the surface density in not uniformly zero outside $r_{\rm vir}$, as it ideally ought to be since the groupfinding algorithm only admits galaxies which are deemed to be bound to a group (i.e. they lie within that group's virial radius). This is due mainly to the scatter in the mass estimates, which translates into a scatter in $r_{\rm vir}$ so that there is uncertainty in the radial scaling of the groups. We assess the impact of this effect in Appendix A2.

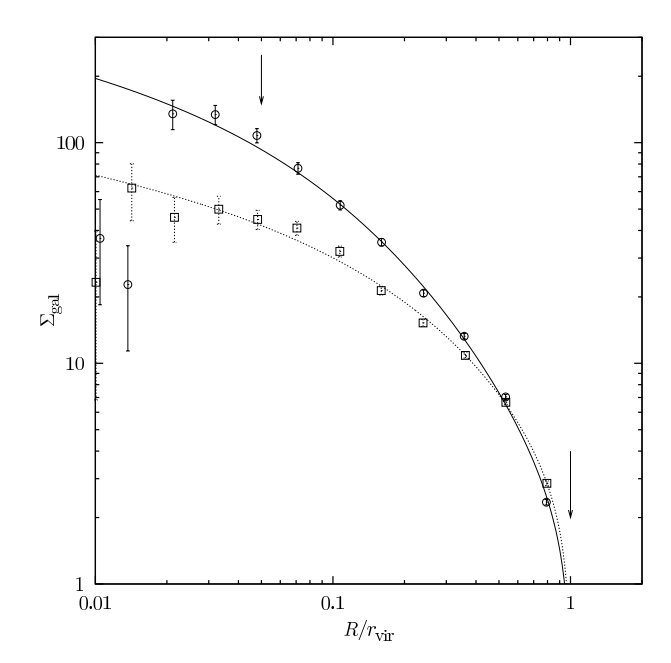


Figure 5. As Fig. 4 but showing separately the results for red (circles) and blue (squares) galaxies. Red galaxies have a more concentrated profile than blue galaxies, and dominate the number counts towards the group centre.

5.1 Profile fitting

Obtaining an analytic fit to the observed profiles will greatly facilitate their use in the halo model. Simulations suggest that dark matter halos obey a universal density profile of the form (Navarro, Frenk & White 1997)

$$\rho(r) = \frac{\rho_s}{r/r_s (1 + r/r_s)^2}$$
 (18)

where $r_{\rm s}$ is a characteristic scale radius, and $\rho_{\rm s}$ sets the amplitude of the profile. This NFW profile is often alternatively expressed in terms of the concentration parameter, $c=r_{\rm vir}/r_{\rm s}$. While there is no physical prerequisite that galaxies should follow the same profile as the dark matter, similar previous studies (e.g. Lin, Mohr & Stanford 2004) have found the NFW profile to provide a good fit to the radial distribution of galaxies, and it therefore constitues the most promising initial guess for the profile.

In order to attempt fitting of the NFW profile to our observations we require its plane projection,

$$\Sigma(R) = 2 \int_{R}^{r_{\text{max}}} \rho(r) \frac{r \, dr}{\sqrt{r^2 - R^2}}.$$
 (19)

In the case $r_{\rm max}=\infty$, equation 19 has an analytic solution (e.g. Bartelmann 1996), but we require $r_{\rm max}=r_{\rm vir}$ since we assume the profile to be truncated at the virial radius. We therefore derive the projected surface density profile numerically from equation 19, with the integration region bounded at the virial radius.

Nagai & Kravtsov (2005) discuss the problem of degeneracy between the concentration parameter and amplitude, ρ_s , of the NFW profile. They suggest that the amplitude be re-expressed in terms of the total number of galaxies contained within the virial radius:

Table 3. Best-fitting NFW concentration parameters. Errors are 1-sigma, marginalized over the probability distribution of the other fitted parameter. $N_{\rm vir}$ represents the average number of galaxies within $r_{\rm vir}$ per group (above the minimum absolute magnitude $M_{b_{\rm J,com}} - 5\log_{10}h = -17.5$).

| | $N_{ m vir}$ | $c = r_{\rm vir}/r_{\rm s}$ |
|--------------|----------------|-----------------------------|
| All galaxies | 39.8 ± 0.8 | 2.4 ± 0.2 |
| Red | 21.7 ± 0.6 | 3.9 ± 0.5 |
| Blue | 18.2 ± 0.5 | 1.3 ± 0.2 |

$$N_{\rm vir} = \int_0^{r_{\rm vir}} \rho(r) \, 4\pi r^2 dr = 4\pi \rho_{\rm s} r_{\rm vir}^3 \frac{g(c)}{c^3}$$
 (20)

where $g(c) = \ln(1+c) - c/(1+c)$. Nagai & Kravtsov (2005) were interested in fitting to simulated data for which $N_{\rm vir}$ could be trivially obtained, reducing the problem to a one-parameter fit. The peculiar velocity distortions in the 2dF redshifts make it impossible to determine $N_{\rm vir}$ reliably for the 2PIGGs, hence we are forced to allow the amplitude of the profile to be a second free parameter. We prefer to use this form none the less, since c is far less degenerate with $N_{\rm vir}$ than it is with $\rho_{\rm s}$, and we find $N_{\rm vir}$ a more intuitive parametrization of the amplitude.

As discussed above, the reliability of the galaxy surface density measurements deteriorates towards the centre of the groups. We therefore restrict the profile fitting to points in the range $0.05 < R/r_{\rm vir} < 1.0$. We find projected NFW profiles are capable of describing the observed profiles very well over the radial range fitted, both for the separate blue and red galaxy profiles and the combined galaxy profile. The best-fitting NFW profiles are overlaid on the data in Figs 4 and 5, and the concentration parameters are given in Table 3. Fig. 6 shows the joint probability distribution for the NFW concentration parameter and amplitude fitted to the data for all galaxies; we find there to be no strong degeneracy between the two parameters.

It is a non-trivial assumption that stacking projected NFW profiles with a range of concentration parameters should result in a composite profile that is still NFW in shape, and which has a concentration parameter indicative of the 'average' of the underlying sample. We therefore test this assumption in Appendix A. For a lognormal distribution of c we find that the composite profile retains the NFW shape, but it has a concentration parameter which is lower than the median c of the underlying sample. The severity of the effect increases as the distribution of c becomes wider.

The best-fitting concentration parameters we give in Table 3 are broadly consistent with the analyses of galaxy clusters in the K-band of the 2 Micron All-Sky Survey by Lin et al. (2004) who obtain $c=2.90^{+0.21}_{-0.22}$, and of 14 CNOC clusters by Carlberg et al. (1997) and van der Marel et al. (2000) who find c=3.7 and 4.2 respectively. Hansen et al. (2004) find c=1-3 for photometrically identified clusters in the SDSS.

We caution that the close-pair incompleteness effects described above mean that we cannot reliably constrain the radial distribution for $R < 0.05 r_{\rm vir}$, so it is impossible, for example, to determine whether the profile is cuspy or flat-cored at its centre. Furthermore, a number of effects, some of which we have already mentioned, are expected to cause the

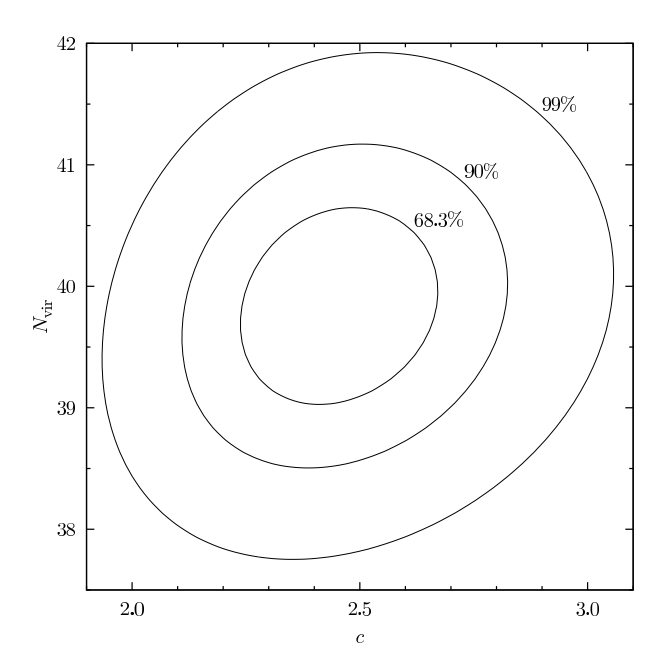


Figure 6. Contours of χ^2 for the concentration parameter and amplitude of the NFW profile fitted to the projected galaxy density profile for all galaxies. Marginalized percentage confidence levels are indicated

measured concentration parameters to be depressed relative to the true value:

- (i) stacking groups (Appendix A),
- (ii) the uncertainty in the radial scaling of groups (Appendix A2),
- (iii) if we are still affected by close-pair incompleteness despite the angular diameter selection we have used, and
- (iv) if there are discrepancies between the position of the 'central' galaxy and the 'true' group centre.

5.2 Mass dependence

The mean concentration parameter of dark matter halos in simulations is found to be a decreasing function of mass, typically modelled as a power law, $c = c_0 \left(M/M_* \right)^{-\lambda}$ with $\lambda \sim 0.1$ and $c_0 \sim 10$ (e.g. Bullock et al. 2001).

Fig. 7 shows the measured concentration parameter against group mass for red and blue galaxies separately, and for the combined sample. These values were obtained by stacking groups within mass bins, and fitting NFW profiles as above. The results suggest a detection of a slight decrease in c with mass, but the trend is barely significant. When calculating halo model-based correlation functions in the following section, we therefore choose to incorporate no mass-dependence in the radial galaxy distribution; we confirm the safety of this assumption below in Section 6.2.

The comparison with the results of Bullock et al. (2001) reveals that, even for the red galaxy distribution, we find the galaxy radial distributions to be significantly less concentrated than those of average dark matter haloes in simulations (but beware the caveats at the end of Section 5.1). The suggestion of a negative correlation of concentration with group mass is in qualitative agreement with the re-

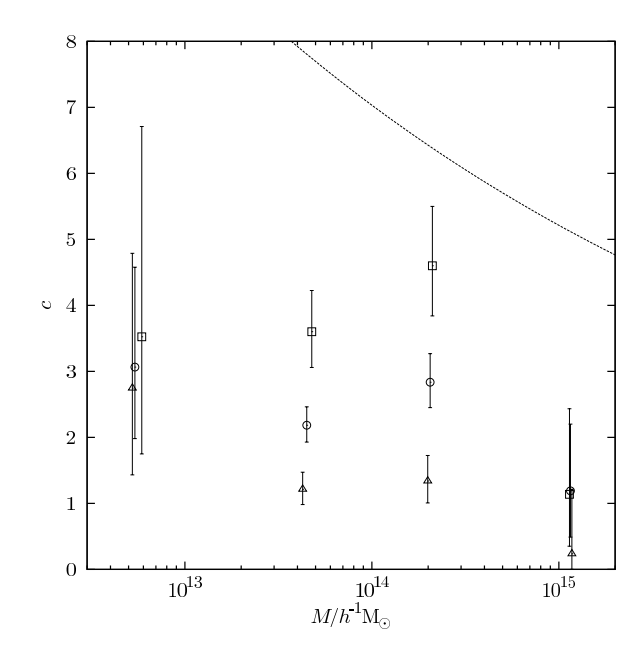


Figure 7. Variation of group concentration parameter with mass, for red (squares), blue (circles), and all galaxies (triangles). For comparison, the dashed line shows the trend in the mean concentration parameter of dark matter haloes in simulations (due to Bullock et al. 2001).

sults of Hansen et al. (2004), who find c to be a decreasing function of galaxy occupation number.

6 PREDICTING CORRELATION FUNCTIONS

Armed with the observations of the previous sections, we are now equipped to calculate the halo model predictions for the correlation function. Hawkins et al. (2003) and Madgwick et al. (2003) have measured the two-point correlation functions for the full 2dFGRS sample and for red and blue subsamples. Care must be taken to ensure a fair, likefor-like comparison, since the correlation function is known to depend on redshift and luminosity (e.g. Zehavi et al. 2002; Norberg et al. 2002a). For this reason, the observed correlation functions are labelled by their effective luminosity and effective redshift. These effective quantities are pairweighted measures, since the correlation function is based on counting pairs of galaxies; hence, for example, the effective redshifts – $z_s = 0.15$ for the all-galaxy sample, and $z_s = 0.11$ for both the red and blue galaxy samples - are somewhat higher than the median redshifts of the samples. We use these redshifts when calculating the halo model correlation functions for the respective populations via the formalism of Section 2.

In the case of the luminosity, the situation is complicated by the fact that the 2dF samples are flux-limited, whereas the halo model formalism effectively assumes volume-limiting. For a volume-limited sample the effective luminosity is identical to the mean luminosity. The minimum luminosity (required by equation 14) is therefore determined by solving

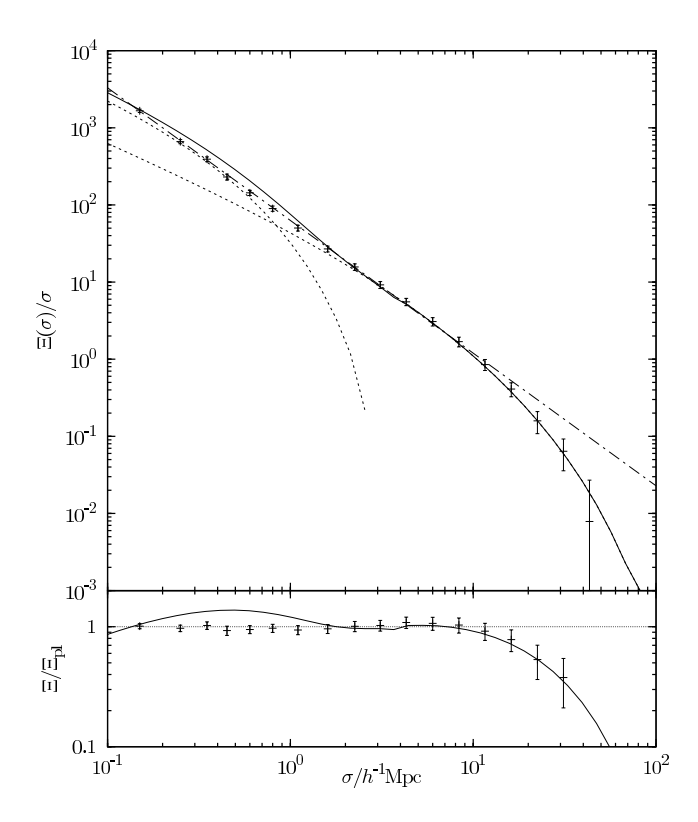


Figure 8. Projected two-point correlation function for galaxies of all types. Data points represent the observed correlation function of Hawkins et al. (2003) and the dot-dashed line is their power-law fit to these points. The solid line is our halo model-based prediction, and the short-dashed lines show the contributions from the individual one- and two-halo terms in the model. The lower panel shows the same data normalized by the power-law fit to the observations.

$$L_{\rm s} = \frac{\int_{L_{\rm min}}^{\infty} L \ \phi(L) \ dL}{\int_{L_{\rm min}}^{\infty} \phi(L) \ dL}, \tag{21}$$

for $L_{\rm min}$. The effective luminosities of the samples used by Hawkins et al. (2003) and Madgwick et al. (2003) are, using $M^* - 5\log_{10}h = -19.66$: all galaxies, $L_{\rm s} = 1.4L_*$; red, $L_{\rm s} = 1.26L_*$; blue, $L_{\rm s} = 0.95L_*$. The resulting limiting absolute magnitudes are $M_{b_{\rm J},\rm com} - 5\log_{10}h = -19.25, -19.04, -19.50$ for red, blue and all galaxies respectively. These limits have been used in determining the halo occupation distribution of the 2PIGG groups (Section 4), and the number densities of the galaxy populations (Table 2).

In order to negate the effect of redshift distortions in the observed correlation functions we use the radial projection,

$$\frac{\Xi(\sigma)}{\sigma} = \frac{2}{\sigma} \int_{\sigma}^{\infty} \frac{\xi(r) \ r \ dr}{(r^2 - \sigma^2)^{1/2}} \ . \tag{22}$$

In Figs 8, 9 and 10 we compare the halo model predictions with the observed projected correlation functions.

In producing these halo model correlation functions we have simply used the best-fitting halo profiles and occupation distributions, deliberately making no attempt to fit to the observed correlation function data. We find that the model successfully recovers the approximate shape and amplitude of the observed correlation functions across the

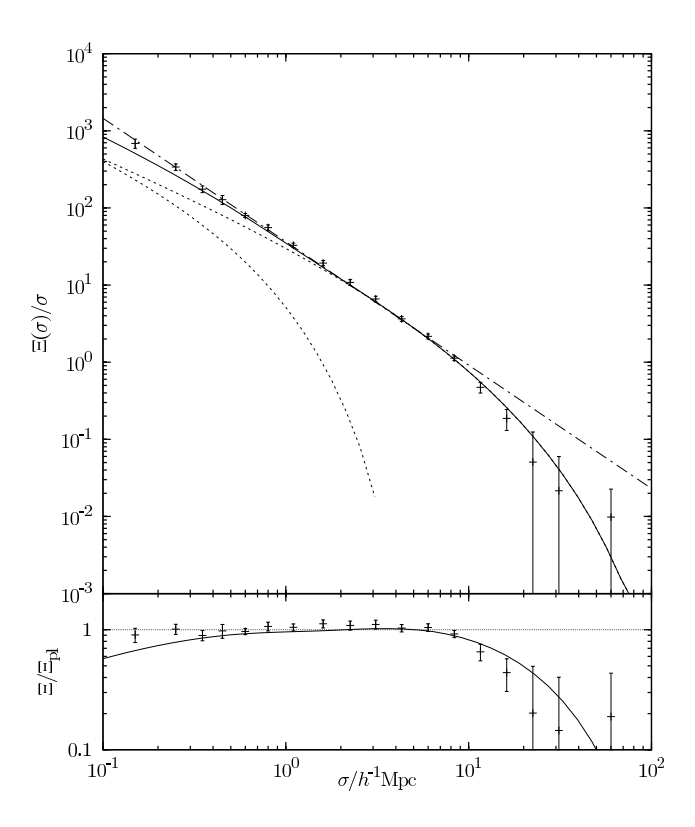


Figure 9. As Fig. 8, but for blue galaxies only, and using the observed correlation function data of Madgwick et al. (2003).

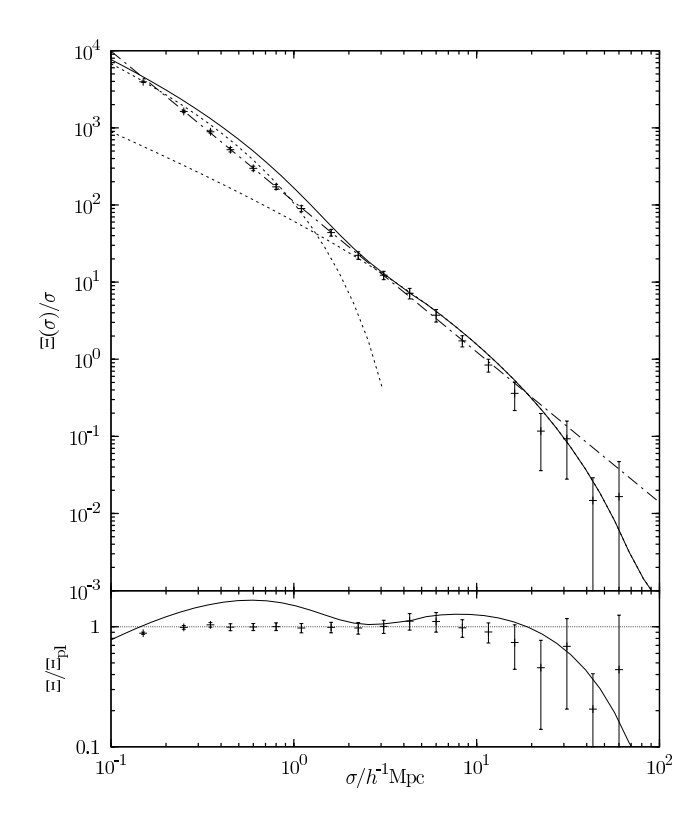


Figure 10. As Fig. 9, but for red galaxies only.

Table 4. Galaxy bias parameters predicted by the halo model. Note that the effective luminosities and redshifts differ between the three galaxy samples.

| | $b_{ m gal}(L_{ m s},z_{ m s})$ | $b_{\mathrm{gal}}(L_*,0)$ |
|--------------|---------------------------------|---------------------------|
| All galaxies | 1.05 | 0.92 |
| Red | 1.23 | 1.12 |
| Blue | 0.85 | 0.81 |

range of distance scales considered. In particular, the model correlation functions trace the obvious divergence from the power-law form at large scales. The different observed HODs and halo profiles of red and blue galaxies derived in Sections 4 and 5 are seen to give rise to the expected relative strengths of correlations on small scales, although the halo model predictions do show significant deviations from the power-law form on these scales.

6.1 Galaxy bias on large scales

On large scales the differences in the correlation functions of the different galaxy classes are encapsulated in the galaxy bias parameter (equation 10). To allow comparison with other results, we correct the galaxy bias parameter for redshift and luminosity dependence via

$$b_{\rm gal}(L,0) = b_{\rm gal}(L,z_{\rm s})D(z_{\rm s})$$
 (23)

and

$$b_{\rm gal}(L,0)/b_{\rm gal}(L_*,0) = 0.85 + 0.15(L/L_*).$$
 (24)

The first relation follows from the assumption that galaxy clustering evolves weakly over this redshift range (i.e. $\sigma_{8,\mathrm{gal}}$ remains approximately constant). The second is found from correlation function analysis by Norberg et al. (2001). The predicted galaxy bias factors are in Table 4. Lahav et al. (2002) have measured the galaxy bias factor by combining the 2dFGRS galaxy power spectrum with the post-WMAP CMB data and found

$$b_{\rm gal}(L_*,0) \approx 0.96 \pm 0.08,$$
 (25)

in good agreement with our predicted value for all galaxies: $b_{\rm gal}(L_*,0)=0.92.$

Furthermore, the relative bias between our red and blue samples, $b_{\rm red}/b_{\rm blue}=1.4$, is in excellent agreement with that found by Cole et al. (2005), who measure the power spectra for red and blue 2dFGRS subsamples defined by a colour cut at $b_{\rm J}-r_{\rm F}=1.07$.

6.2 Sensitivity to parameters

The halo bias factor, b(M), (equation 8) is a monotonically increasing function of mass, with the lowest mass haloes in fact being anti-biased. The galaxy bias factor predicted by the halo model (equation 11) will therefore be controlled by the relative occupation of high to low mass groups: thus, since the red galaxies have a steeper $\langle N|M\rangle$ than the blue, they also have a greater large-scale bias factor.

The differences on small scales are, in principle, due to the different radial profiles as well as the relative halo occupation numbers of the galaxy classes. However, it turns out that on the scales we are currently able to access observationally (and given the observational results of the previous sections) the correlation function is much more sensitive to the differences in the halo occupation distribution (see also Sheth et al. 2001; Berlind & Weinberg 2002; Scranton 2003). For example, substituting the dark matter concentration parameter relation of Bullock et al. (2001, see Section 5.2), in place of the observed values has a perceptible effect only on scales $r\lesssim 3\times 10^{-1}{\rm Mpc}/h$.

As we explain in Section 4.2, the HOD for low mass groups is unconstrained by the observations. In consequence, we are forced to assume an extrapolation of the high mass HOD to low masses. The shape of the intra-halo term of the correlation function is strongly dependent on the particular form assumed for the halo occupation distribution at low group masses, but the overall amplitude is robust to such details, being dominated by the contribution from galaxy pairs in high-mass haloes. Berlind & Weinberg 2002 demonstrate the contributions to $\xi(r)$ from galaxy pairs as a function of halo mass: in general lower mass haloes become influential on smaller scales. By using a more sophisticated extrapolation to low masses it is possible to produce a halo model correlation function which more faithfully reproduces the power-law form on small scales. For example, we show in Fig. 11 the correlation function for all galaxies produced by using a halo occupation distribution of the form

$$\langle N|M\rangle = \begin{cases} (M/M_0)^{\beta} & (M \geqslant M_0) \\ 1 & (M_{\text{cut}} \leqslant M < M_0) \\ 0 & (M < M_{\text{cut}}) \end{cases}$$
 (26)

with M_0 and β as given in Table 1, and introducing an ad hoc sub-Poisson distribution at low masses:

$$\alpha(M) = \begin{cases} 1 & (M \geqslant M_0) \\ 0.2 & (M < M_0) \end{cases} . \tag{27}$$

As described in Section 4.2, we constrain $M_{\rm cut}$ by matching the observed number density. For this choice of HOD we obtain a much more realistic $M_{\rm cut} = 1.4 \times 10^{12} h^{-1} {\rm M}_{\odot}$. Both this and our simplest possible HOD (equation 16) are entirely consistent with our observations, and are successful at recovering the amplitude of the correlation function. However, the more sophisticated form gives a much better fit to the observations on small scales.

7 DISCUSSION

Motivated by the halo model, we have used the 2dF Percolation-Inferred Galaxy Group catalague to make direct observational estimates of the distribution functions of galaxies within and amongst haloes. We have found a projected NFW profile provides a good fit to the composite projected surface density of galaxies in red and blue subclasses, and for the combined sample. The radial distribution of the red galaxies was found to be the most concentrated towards the group centre, but, even for these, the concentration is significantly lower than for dark matter haloes measured in simulations.

We have shown that at high masses the mean occupation number of the 2PIGGs with red, blue, and all galaxies can be described by a power-law in the mass, with the number of red galaxies increasing most steeply with the mass.

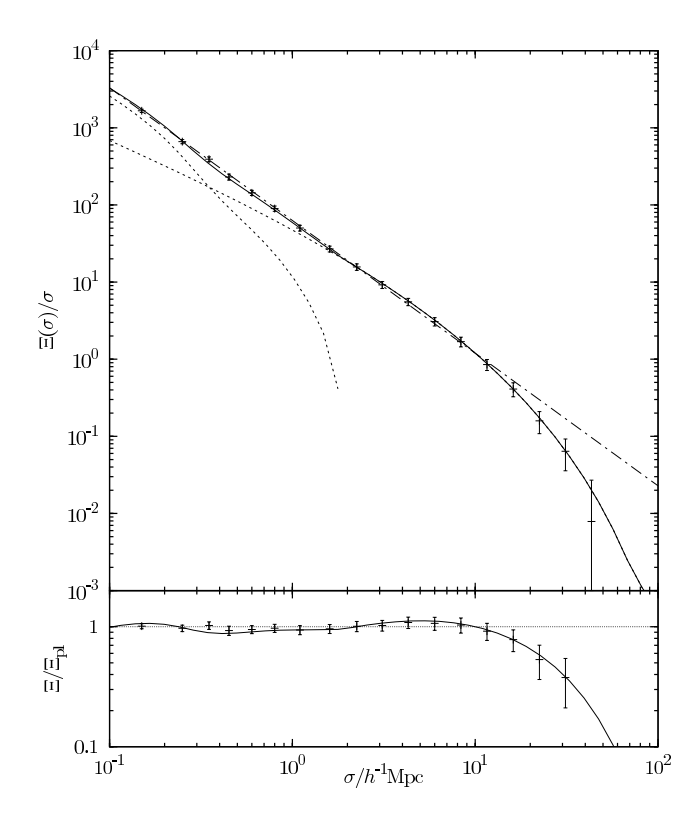


Figure 11. As Fig. 8, but the halo model predictions are based on the more sophisticated HOD described by equations 26 and 27. This form of the HOD better reproduces the power-law on small scales, while still being consistent with the observational constraints of Section 4.

The difficulty of obtaining reliable dynamical mass estimates for groups with low occupation numbers made it difficult to constrain the halo occupation distribution in this regime.

These observations have allowed us to test the halo model against fully self-consistent observations: the same 2dFGRS galaxy populations used to compile the 2PIGG catalogue have previously had their correlation functions directly determined. Despite the uncertainty regarding the form of the halo occupation distribution at low halo masses, the halo model proves successful at reproducing the near power-law form of the galaxy correlation functions. Most impressively, the model also succesfully recovers the relative biasing of the red and blue subpopulations. In agreement with Sheth et al. (2001), we identify the halo occupation number, $\langle N|M\rangle$, as the dominant factor contributing to the differences in the correlation functions of red and blue galaxies: the HOD for red galaxies gives a greater weighting to high-mass haloes leading to a stronger clustering signal on all scales. The differences in the radial distributions of the galaxies in groups are found to be relatively unimportant on the distance scales we are presently able to access observationally, but do begin to exert influence at the smallest scales considered.

There are of course any number of forms which could be chosen for the extrapolation of the HOD to low mass (see for example, Kravtsov et al. 2004; Sheth & Diaferio 2001; Scranton 2003; Magliocchetti & Porciani 2003). We have shown that the power-law form of the observed correlation

functions does place constraints on this extrapolation. However, in the intra-halo term there is certainly degeneracy between $\alpha(M)$ and $\langle N|M\rangle$, so it is unlikely that the two-point correlation can be used to constrain a unique solution. Direct measurement of the HOD for low-mass haloes requires much improved mass estimates, and represents a difficult observational challenge. Higher order clustering statistics represent a more stringent test for the halo model, and offer the possibility of indirectly constraining the low-mass HOD in a more model-independent fashion than is possible from the two-point function alone (e.g. Ma & Fry 2000; Scoccimarro et al. 2001; Wang et al. 2004; Fosalba, Pan & Szapudi 2005).

ACKNOWLEDGMENTS

We gratefully acknowledge the assistance of Vince Eke, Josh Frieman, Yehuda Hoffman and Frank van den Bosch. We also thank our referee, Ravi Sheth, for many useful suggestions. AAC is supported by an Isle of Man Department of Education Postgraduate Studies Grant. OL acknowledges a PPARC Senior Research Fellowship.

REFERENCES

Bartelmann M., 1996, A&A, 313, 697

Benson A. J., Cole S., Frenk C. S., Baugh C. M., Lacey C. G., 2001, MNRAS, 327, 1041

Berlind A. A., Weinberg D. H., 2002, ApJ, 575, 587

Bullock, J. S., Kolatt, T. S., Sigad, Y., Somerville, R. S., Kravtsov, A. V., Klypin, A. A., Primack, J. R., Dekel, A., 2001, MNRAS, 321, 559

Carlberg R. G., et al., 1997, ApJ, 485, L13

Casas-Miranda R., Mo H. J., Sheth R. K., Boerner G., 2002, MNRAS, 333, 730

Cole S. & The 2dFGRS team, 2005, preprint (astro-ph/0501174)

Cooray A., Sheth R. K., 2002, Phys. Rep., 371, 1

Croton D. J. & The 2dFGRS team, 2005, MNRAS, 356, 1155

Dressler A., 1980, ApJ, 236, 351

Efstathiou G. & The 2dFGRS team, 2002, MNRAS, 330, $29\,$

Eke V. R., Cole S., Frenk C. S., 1996, MNRAS, 282, 263

Eke V. R. & The 2dFGRS team, 2004a, MNRAS, 348, 866 Eke V. R. & The 2dFGRS team, 2004b, MNRAS, 355, 769

Fosalba P., Pan J., Szapudi I., 2005, preprint (astro-ph/0504305)

Goto T., Yamauchi C., Fujita Y., Okamura S., Sekiguchi M., Smail I., Bernardi M., Gomez P. L., 2003, MNRAS, 346, 601

Hansen S. M., McKay T. A., Wechsler R. H., Annis J., Sheldon E. S., Kimball A., 2004, preprint (astro-ph/0410467)
Hawkins E. & The 2dFGRS team, 2003, MNRAS, 346, 78
Jing Y. P., 2000, ApJ, 535, 30

Kauffmann G., Colberg J. M., Diaferio A., White S. D. M., 1999, MNRAS, 303, 188

Kravtsov A. V., Berlind A. A., Wechsler R. H., Klypin A. A., Gottlöber S., Allgood B., Primack J. R., 2004, ApJ, 609, 35

Lahav O. & The 2dFGRS team, 2002, MNRAS, 333, 961

Lin Y.-T., Mohr J. J., Stanford S. A., 2004, ApJ, 610, 745Ma C., Fry J. N., 2000, ApJ, 543, 503

Madgwick D. S. & The 2dFGRS team, 2002, MNRAS, 333, 133

Madgwick D. S. & The 2dFGRS team, 2003, MNRAS, 344, 847

Magliocchetti M., Porciani C., 2003, MNRAS, 346, 186

 $Mo\ H.\ J.,\ White\ S.\ D.\ M.,\ 1996,\ MNRAS,\ 282,\ 347$

Nagai D., Kravtsov A. V., 2005, ApJ, 618, 557

Navarro J. F., Frenk C. S., White S. D. M., 1997, ApJ, 490, 493

Neyman J., Scott E. L., 1952, ApJ, 116,144

Norberg P. & The 2dFGRS team, 2001, MNRAS, 328, 64

Norberg P. & The 2dFGRS team, 2002a, MNRAS, 332, 827

Norberg P. & The 2dFGRS team, 2002b, MNRAS, 336, 907

Padilla N. D. & The 2dFGRS team, 2004, MNRAS, 352, 211

Peacock J. A., Smith R. E., 2000, MNRAS, 318, 1144

Peebles P. J. E., 1980, The Large Scale Structure of the Universe. Princeton Univ. Press, Princeton NJ

Percival W. J. & The 2dFGRS team, 2001, MNRAS, 327, 1297

Postman M., Geller M. J., 1984, ApJ, 281, 95

Press W. H., Schechter P., 1974, ApJ, 187, 425

Scherrer R. J., Bertschinger E., 1991, ApJ, 381, 349

Scoccimarro R., Sheth R. K., Hui L., Jain B., 2001, ApJ, 546, 20

Scranton R., 2003, MNRAS, 339, 410

Seljak U., 2000, MNRAS, 318, 203

Sheth R. K., Diaferio A., 2001, MNRAS, 322, 901

Sheth R. K., Tormen G., 1999, MNRAS, 308, 119

Sheth R. K., Diaferio A., Hui L., Scoccimarro R., 2001, MNRAS, 326, 423

Spergel D. N. et al., 2003, ApJS, 148, 175

Tegmark M. et al., 2002, ApJ, 571, 191

van den Bosch F. C., Yang X., Mo H. J., 2003, MNRAS, 340, 771

van den Bosch F. C., Yang X., Mo H. J., Norberg P., 2005, MNRAS, 356, 1233

van der Marel R. P., Magorrian J., Carlberg R. G., Yee H. K. C., Ellingson E., 2000, AJ, 119, 2038

Wang Y., Yang X., Mo H. J., van den Bosch F. C., Chu Y., 2004, MNRAS, 353, 287

Yang X., Mo H. J., van den Bosch F. C., Jing Y. P., 2005a, MNRAS, 356, 1293

Yang X., Mo H. J., van den Bosch F. C., Jing Y. P., 2005b, MNRAS, 357, 608

Yang X., Mo H. J., Jing Y. P., van den Bosch F. C., 2005c, MNRAS, 358, 217

Zehavi I., Blanton M. R., Frieman J. A. et al., 2001, ApJ, 571, 172

APPENDIX A: STACKING GROUPS

In order to allow accurate measurement of the galaxy radial distribution it is necessary to combine many groups so as to improve the statistics. Even the largest groups in the 2PIGG catalogue do not have sufficient galaxy members to allow the concentration parameter to be well constrained for individual groups.

The groups are scaled by their virial radius. However,

Table A1. Results from fitting NFW profiles to stacked profiles having concentration parameters drawn from lognormal distributions with the given median (\bar{c}) and width (σ_c) . The concentration parameter of the best-fitting NFW profile, $c_{\rm fit}$, is found to be a fair indicator for the mode of the underlying distribution.

| \bar{c} | σ_c | $c_{ m fit}$ | $c_{ m mode}$ |
|-----------|------------|--------------|---------------|
| 10 | 0.1 | 9.79 | 9.90 |
| 10 | 0.2 | 9.19 | 9.61 |
| 10 | 0.5 | 6.18 | 7.79 |
| 10 | 1.0 | 2.22 | 3.68 |
| 5 | 0.1 | 4.91 | 4.95 |
| 5 | 0.2 | 4.66 | 4.80 |
| 5 | 0.5 | 3.31 | 3.90 |
| 5 | 1.0 | 1.34 | 1.84 |
| | | | |

NFW profiles with different concentration parameters are not self-similar when scaled in this way (scaling by $r_{\rm s}$, on the other hand, does produce self-similar profiles, but this approach is not practical since estimating $r_{\rm s}$ is non-trivial). It is not clear therefore that the resulting profile will retain the NFW form, or that the concentration parameter thus obtained will be at all indicative of the 'average' concentration of the groups in the sample.

We do not have any indication of the expected distribution of the concentration parameter for galaxy groups, due to the difficulty in measuring the profile for individual groups. For dark matter haloes, simulations (e.g. Jing 2000; Bullock et al. 2001) suggest that c has a lognormal distribution at fixed halo mass,

$$p(c|M)dc = \frac{1}{\sqrt{2\pi}\sigma_c} \exp\left[-\frac{(\ln c - \ln \bar{c})^2}{2\sigma_c^2}\right] d\ln c \tag{A1}$$

where the median, \bar{c} , contains the only dependence on halo mass (see §A1). Both Jing (2000) and Bullock et al. (2001) find $\sigma_c \sim 0.2$. Although there is no reason to assume that these results apply equally well to the galaxy group profiles, we use this distribution in order to illustrate the effect of stacking profiles with a wide range of concentrations.

Stacking profiles drawn from a distribution p(c) will produce the aggregate profile,

$$\bar{\Sigma}(R) = \int \Sigma(R|c) \ p(c) \ dc. \tag{A2}$$

We have computed this aggregate profile for a range of lognormal distributions, and fitted a projected NFW profile to the result, just as for the real data (i.e. using only the region $0.05 < R/r_{\rm vir} < 1.0$).

The stacked profiles can be well fitted by the NFW profile, even for the widest distributions. However, the concentration parameter of the best-fitting profile is systematically lower than the median of the underlying distribution. Table A1 shows the results for the range of distributions considered.

The disparity between the median and fitted c becomes increasingly significant as the distribution broadens. However, the best-fitting c is found to be a fair indicator for the mode (i.e. peak position) of the underlying lognormal distribution, particularly when the dispersion is relatively low.

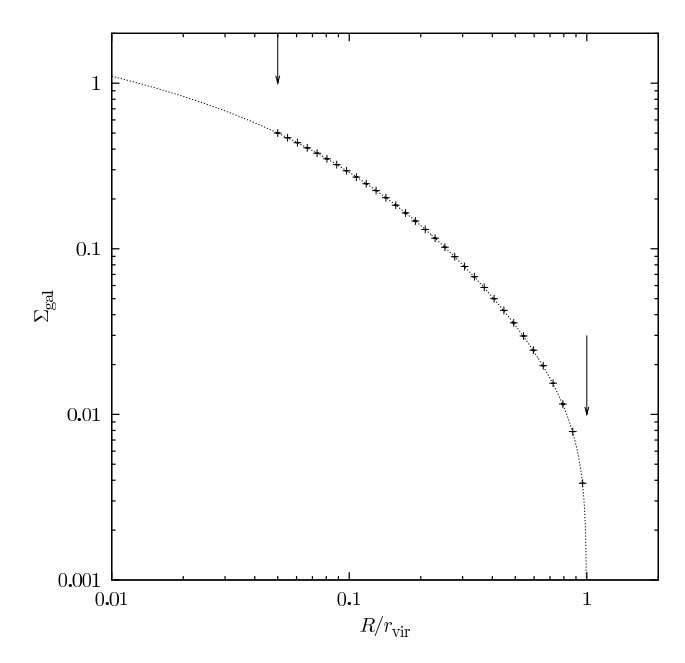


Figure A1. The crosses show the simulted aggregate profile obtained by stacking NFW profiles drawn from a lognormal distribution with median $\bar{c}=5$ and width $\sigma_c=0.2$. The dotted line is the NFW profile which best fits the stacked points; it has c=4.66.

A1 Mass dependence

Bullock et al. (2001) find the median concentration parameter for dark matter haloes to be a function of halo mass: $\bar{c}(M) \approx 9(M/M_*)^{-0.13}$ at z=0. In combination with the mass function, n(M) (equation 5), this allows us to write down the global distribution of c as

$$f(c) = \int p(c|M) \ n(M) \ dM. \tag{A3}$$

Figure A2 shows this global distribution for haloes in the mass range $10^{13} < M/h^{-1}{\rm M}_{\odot} < 10^{16}$, assuming p(c|M) is lognormal with $\sigma_c = 0.2$. The combination with the mass function leads to a slight widening of the distribution, particularly on the low-c tail.

This result clearly depends on the assumption of forms for $\bar{c}(M)$ and p(c|M), both of which we have derived from simulated dark matter haloes. Our observational results (Fig. 7) suggest that $\bar{c}_{\rm gal}$ depends on the host halo mass no more strongly than does the dark matter concentration parameter.

What is most important is that the combination with the mass function has not significantly altered the shape of the distribution, so that the results of Section A still hold when we stack groups covering a wide range of masses, albeit with a slightly wider underlying distribution of c.

A2 Scaling uncertainty

The dynamical masses determined by Eke et al. (2004a) for the 2PIGG groups have a large scatter, particularly for small (low membership) groups. Figure 3 of Eke et al. (2004b) illustrates the dependence of this scatter on group membership. Since low-membership groups are the most abundant

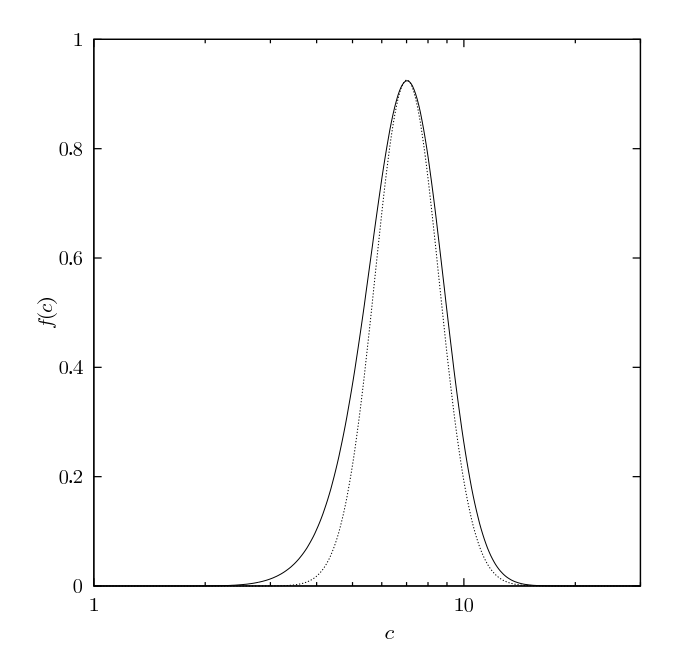


Figure A2. The solid curve is the global distribution of c for dark matter haloes (equation A3). For comparison, the dotted line shows a lognormal distribution with width $\sigma_c = 0.2$ and having the same mode as the global distribution.

in the 2PIGG catalogue, one might expect the scaling error to be dominated by their contribution. Fortunately however, the impact on the stacked profile of groups with a particular membership, N, is proportional to $N \times n(N)$. Thus, although there are many more low-membership groups, the individual groups have proportionally less impact on the stacked profile than a single high-membership group. It turns out that $N \times n(N)$ is nearly independent of N for the 2PIGG catalogue, so the overall scaling error receives roughly equal contributions from all group memberships.

We adopt N=10 as our fiducial point, since the error distribution here is close to average. The distribution of $M/M_{\rm true}$ at N=10 is roughly lognormal with median 1.26 and $\sigma \sim 1.0$. Propagating the error distribution of $M/M_{\rm true}$ through equation 13 implies that $r/r_{\rm true}$ has a lognormal distribution with median 1.08 and $\sigma \sim 0.33$: the $r_{\rm vir} \propto M^{1/3}$ relation means the large scatter in the mass estimates is considerably suppressed, leading to a somewhat narrower distribution of $r/r_{\rm true}$ (Fig. A3).

The aggregate profile obtained by stacking profiles with an uncertain radial scaling is given by

$$\tilde{\Sigma}(R) = \int \Sigma\left(\frac{R}{s} \mid c\right) p(s) ds, \tag{A4}$$

where we have defined the scaling error, $s = r/r_{\text{true}}$, and its probability distribution p(s) which, as we have discussed above, may be approximated by a lognormal distribution. This profile is illustrated in Fig. A4.

The scaling uncertainty has the effect of smoothing the cut-off at the virial radius, just as observed in Section 5, and causes a significant reduction in the measured concentration parameter.

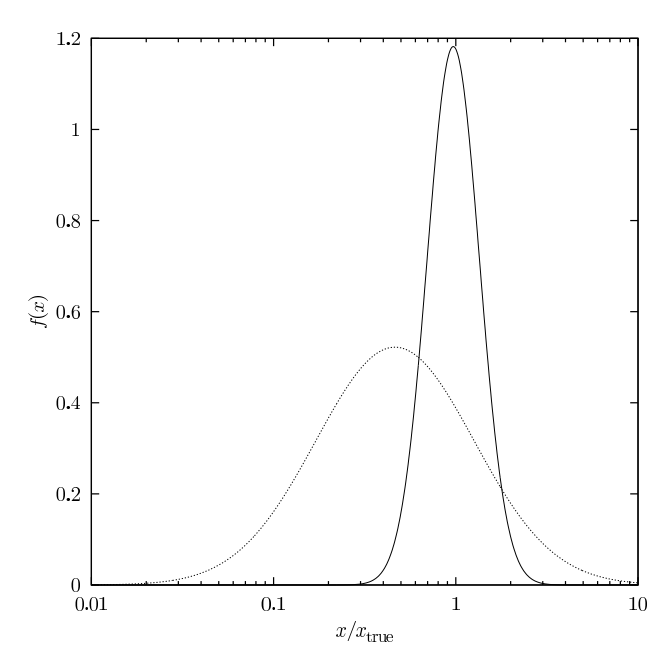


Figure A3. The dotted line is the error distribution in the group mass estimates (derived from equation 12) for groups having N=10 observed galaxy members. Through equation 13 this implies an error distribution in the virial radius, shown by the solid line.

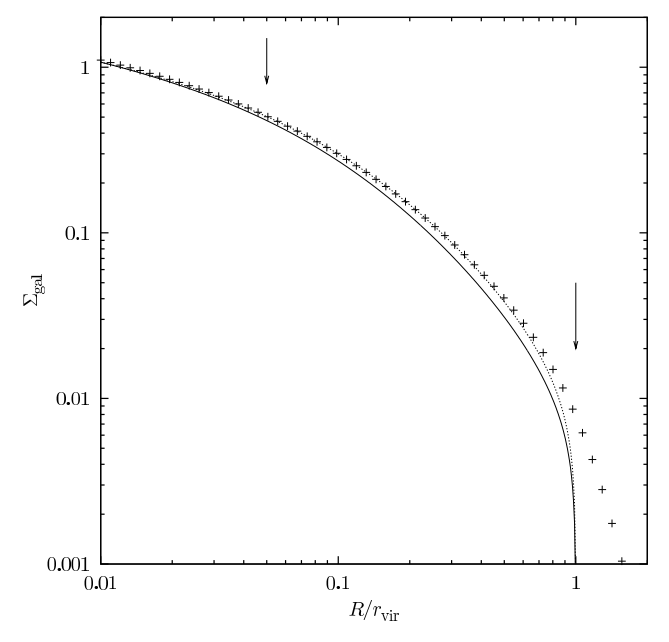


Figure A4. Effect of scaling uncertainty on the aggregate profile obtained by stacking groups. The solid line shows a projected NFW profile with c=5.0. Crosses show simulated data generated by equation A4, assuming the scaling uncertainty described in the text. The dotted line is the NFW profile which best-fits the data; it has c=4.13.